HHS Public Access

Author manuscript

J Control Release. Author manuscript; available in PMC 2017 December 10.

Published in final edited form as:

J Control Release. 2016 December 10; 243: 69–77. doi:10.1016/j.jconrel.2016.09.010.

Intracellular delivery and ultrasonic activation of folate receptor-targeted phase-change contrast agents in breast cancer cells *in vitro*

Joseph P. Marshalek[1], **Paul S. Sheeran**[2], **Pier Ingram**[1], **Paul A. Dayton**[3], **Russell S. Witte**[1], and **Terry O. Matsunaga**[1]

[1]Department of Medical Imaging, University of Arizona, Tucson, Arizona, USA

[2]Physical Sciences Department, Sunnybrook Research Institute, Toronto, Ontario, Canada; Department of Medical Biophysics, University of Toronto, Toronto, Ontario, Canada

[3]Joint Department of Biomedical Engineering, The University of North Carolina and North Carolina State University, Chapel Hill, North Carolina, USA

Abstract

Breast cancer is a diverse and complex disease that remains one of the leading causes of death among women. Novel, outside-of-the-box imaging and treatment methods are needed to supplement currently available technologies. In this study, we present evidence for the intracellular delivery and ultrasound-stimulated activation of folate receptor (FR)-targeted phase-change contrast agents (PCCAs) in MDA-MB-231 and MCF-7 breast cancer cells *in vitro*. PCCAs are lipid-coated, perfluorocarbon-filled particles formulated as nanoscale liquid droplets capable of vaporization into gaseous microbubbles for imaging or therapy. Cells were incubated with 1:1 decafluorobutane (DFB) / octafluoropropane (OFP) PCCAs for 1 hour, imaged via confocal microscopy, exposed to ultrasound (9 MHz, MI = 1.0 or 1.5), and imaged again after insonation. FR-targeted PCCAs were observed intracellularly in both cell lines, but uptake was significantly greater ($p < 0.001$) in MDA-MB-231 cells (93.0% internalization at MI = 1.0, 79.5% at MI = 1.5) than MCF-7 cells (42.4% internalization at MI = 1.0, 35.7% at MI = 1.5). Folate incorporation increased the frequency of intracellular PCCA detection 45-fold for MDA-MB-231 cells and 7-fold for MCF-7 cells, relative to untargeted PCCAs. Intracellularly activated PCCAs ranged from 500 nm to 6 microns (IQR = 800 nm – 1.5 microns) with a mean diameter of 1.15 ± 0.59 (SD) microns. The work presented herein demonstrates the feasibility of PCCA intracellular delivery and activation using breast cancer cells, illuminating a new platform toward intracellular imaging or therapeutic delivery with ultrasound.

Corresponding Author: Terry O. Matsunaga, Electronic Address: tmatsunaga@radiology.arizona.edu, Telephone Number: (520) 626 – 6689.

Keywords

Ultrasound; phase-change contrast agent; microbubble; nanodroplet; perfluorocarbon; decafluorobutane; octafluoropropane; folate receptor; breast cancer

1. Introduction

For women in the United States, breast cancer is the most commonly diagnosed cancer and second leading cause of cancer-related death [1]. With an estimated 1.38 million new breast cancer cases and 458,000 deaths per year worldwide [2], new and unique diagnostic and therapeutic tools are vital for slowing the progression and mortality of this disease.

Ultrasound (US) has been utilized for a broad range of applications in tumor imaging [3, 4, 5, 6, 7] as well as drug and gene delivery [8, 9, 10, 40, 41]. Compared to other imaging paradigms, ultrasound is particularly advantageous as a noninvasive and nonionizing modality. Furthermore, ultrasound is portable and inexpensive, making it well suited for the rapidly evolving state of health care in the 21st century.

Microbubble contrast agents have been investigated for ultrasound imaging of atherosclerosis [11], tumor angiogenesis [12], and other applications of intravascular tumor imaging [5, 7, 13]. Gas-filled microbubbles (MBs) provide high imaging contrast relative to tissue, yet they are restricted to the vasculature by their size (typically 1 – 10 microns). This size limitation can be circumvented using nanoscale phase-change contrast agents (PCCAs), which refers to liquid perfluorocarbon droplets capable of shifting phases into gaseous microbubbles via acoustic droplet vaporization [14]. The PCCA platform is unique in that nanodroplets (50 – 700 nm) can be formulated small enough to potentially extravasate into cancer tissue, target specific biomarkers, and then undergo receptor-mediated endocytosis for intracellular nanoparticle delivery. The application of ultrasound can then trigger acoustic droplet vaporization of intracellular nanodroplets into gaseous microbubbles for imaging or therapy (Figure 1).

The ultrasound PCCA cancer-imaging concept is dependent upon the “leaky” vasculature of tumor tissue. In normal tissue, the maximum particle size for extravasation from the vasculature is roughly 10 nm, while nanoparticles up to 600 nm can escape through the porous tumor endothelium [15]. Tumor vasculature can be highly angiogenic, with abnormal blood vessels characterized by uneven diameter, excessive branching and shunts, and high permeability [16]. The enhanced permeability and retention (EPR) effect facilitates increased accumulation of nanoparticles in tumor tissue, and this passive tumor targeting mechanism is optimized for nanoparticles sized 50 – 250 nm [17]. Another advantage of the PCCA platform is the fact that perfluorocarbon nanodroplets can persist in circulation for significantly longer than microbubbles [18], thus enhancing the likelihood of extravasation and cellular targeting.

Our PCCAs are composed of a perfluorocarbon (PFC) core encapsulated by a lipid membrane, to which ligands can be attached for targeted delivery. In this study, the PFC core was a 1:1 mixture of decafluorobutane (DFB, C_4F_{10}, BP = −2 °C) and octafluoropropane

(OFP, C_3F_8, BP = −37 °C). When isolated in the bulk phase, these low-boiling perfluorocarbons vaporize well below physiological temperatures. However, when encapsulated at the micro- and nanoscale, PCCAs based on these perfluorocarbons exhibit thermal vaporization thresholds as much as 70 °C higher than the bulk boiling point due to the thermodynamic limits of superheat and additional Laplace pressure at these small sizes [19, 20].

PCCA-based ultrasound imaging relies upon the application of acoustic energy to activate nanodroplets into microbubbles. Under FDA ultrasound guidelines, the maximum mechanical index (MI) permitted clinically is 1.9. However, this does not necessarily imply that the clinical use of PCCAs will also be permitted at a maximum of 1.9. Indeed, the guidelines for the use of Definity™ microbubbles recommends a mechanical index less than 0.8 in order to prevent microbubble cavitation [21]. Currently, there are no clinical care guidelines surrounding use of PCCAs, as they are not clinically approved agents. Nonetheless, our approach to generating droplets by condensing microbubbles has some unique strategic advantages that we believe will aid clinical translation – that droplets are formed from the same constitutive components used for clinically approved microbubbles. Before PCCAs can be used clinically, there are still a range of studies required on biodistribution, bioeffects upon activation, and dose tolerance.

Over the past few years, growing interest in PCCAs has launched efforts into understanding the underlying physics and acoustic characteristics of the agents [22]. Pre-clinical studies in large animals (i.e. porcine) have shown that, under limited frequencies and mechanical indices, vaporization and imaging with PCCAs does not seem to produce adverse effects [23]. However, there still needs to be an extensive and systematic treatise on PCCA safety and bioeffects over a range of MIs, investigating both the role of frequency and pressure across the entire diagnostic range.

Acoustic droplet vaporization of perfluorocarbon PCCAs has been studied using mechanical indices greater than 0.4 and ultrasound frequencies ranging from 5 – 40 MHz [19, 24, 25, 26, 27, 28]. In general, as the boiling point of a perfluorocarbon increases, more acoustic energy is required for vaporization. This introduces a trade-off between nanodroplet thermal stability and sensitivity to acoustic droplet vaporization. In this study, we applied ultrasound at 9 MHz with a mechanical index of 1.0 or 1.5. Previous work has demonstrated that 1:1 DFB/OFP PCCAs are susceptible to acoustic droplet vaporization within these parameters [26].

In order to promote cellular internalization, we decorated folate to the PCCA shell in order to target folate receptor-alpha (FR-α), which is overexpressed on the surface of breast, ovarian, cervical, and colorectal cancer cells and relatively absent from normal tissues [29]. Previous studies have shown that folate receptor overexpression is associated with worse clinical outcomes in breast cancer patients [30, 31]. Hartmann et al. showed that 81% of breast tumors with strong FR-α expression recurred, compared to 38% recurrence for tumors with weak FR-α expression [31]. Necela et al. demonstrated that FR-α overexpression is associated with increased folate uptake and increased growth of breast cancer cells [32], implying FR-mediated folate uptake as a potential tumor-promoting

mechanism. The association between FR-α overexpression and poor prognosis suggests that FR-targeting can be used to detect or treat high-risk breast tumors.

In addition to its affordability, the folate ligand is an appealing avenue for targeted delivery due to its high binding affinity and internalization frequency for the folate receptor [33]. The two breast cancer cell lines analyzed in this study were MDA-MB-231 and MCF-7, both of which express folate receptor, although MDA-MB-231 cells express FR-α to a greater extent than MCF-7 cells [34, 35]. Recent efforts to quantify folate receptor isoform expression on the surface of breast cancer cells has shown that MDA-MB-231 cells have 1.76 times more FR-α expression relative to MCF-7 cells [35]. Folate receptor-targeted nanoparticles have been investigated for magnetic resonance imaging [34] and photoacoustic imaging [36] of breast tumors. In addition to imaging agents, targeted nanoparticles can deliver gene vectors or drugs to cancer cells, thereby maximizing the therapeutic payload and limiting off-target effects. Folate receptor-targeted nanovehicles have been used to deliver siRNA [37] and chemotherapeutic drugs [38, 39, 40, 41, 42] intracellularly within MDA-MB-231 and MCF-7 breast cancer cells. Nanoparticles ranging from 50 – 400 nm are capable of folate receptor-mediated endocytosis [36, 37, 40, 44], which overlaps with the sizing distribution of our 1:1 DFB/OFP nanodroplet formulation used in the present study [26]. For both MDA-MB-231 and MCF-7 breast cancer cells, one hour has proven sufficient for intracellular accumulation of nanoparticles via the folate receptor pathway [34, 36].

Following folate receptor-mediated nanoparticle uptake by cancer cells, ultrasound has been used to trigger drug release from eLiposomes [43] or polymersomes [44]. However, the ultrasound PCCA platform has not yet been applied for targeted molecular imaging of breast cancer. In this *in vitro* proof-of-principle study, we provide evidence of folate receptor-mediated intracellular delivery and ultrasonic activation of PCCAs using breast cancer cells.

2. Materials and Methods

2.1 Tissue Culture

Human breast cancer cell lines MDA-MB-231 and MCF-7 (obtained from the Experimental Mouse Shared Services at The University of Arizona Cancer Center) were cultured in RPMI-1640 Medium and Dulbecco's Minimum Eagle Medium, respectively, supplemented with 10% fetal bovine serum and 1% antibiotics (100 μg/mL penicillin-streptomycin). The cells were grown in 75 cm^2 culture flasks (Sarstedt, Numbrecht, Germany) and maintained at 37 °C in an incubator containing 5% CO_2. Two days prior to confocal imaging, cells were plated on a 50 mm diameter circular d-polylysine coated culture dish with a No. 1.5 coverslip attached over a small hole in the bottom dish (MatTek Corp., Ashland, MA). At the time of imaging, cells were roughly 40 – 60% confluent across the coverslip.

2.2 PCCA Formulation

PCCA sample preparation has been adapted from previously described literature methods [45], with the following modifications and clarifications. The lipid coat was prepared as a colloidal dispersion by dissolving a 9:1 ratio of dipalmitoylphosphatidylcholine (DPPC) and 1,2-dipalmitoyl-sn-glycero-3-phosphoethanolamine-N-{methoxy(polyethylene

glycol)-2000] (DPPE-PEG-2000) (Avanti Polar Lipids, Alabaster, AL) in a solution of normal saline, propylene glycol, and glycerol (16:3:1, v:v) for a total lipid concentration of 1 mg/mL. The lipids were first dissolved in propylene glycol by heating to approximately 60 °C. Once dissolved, normal saline was slowly added, and heating was maintained until the lipid colloid remained opalescent in appearance. Finally, the remaining glycerol was added with heating so as to maintain the opalescent appearance.

For the FR-targeted PCCA formulation, folate bioconjugate ligand (Avanti Polar Lipids, Alabaster, AL) (Figure 2) was added to the lipid emulsion at a concentration of 2 mol %. Untargeted PCCAs were formulated without folate incorporation. A volume of 1.5 mL of the lipid mixture was added to a 3 mL glass vial (Wheaton Industries, Millville, NJ), and 1,1'-dioctadecyl-3,3,3',3'- tetramethylindocarbocyanine perchlorate (DiI, Invitrogen, Eugene, OR) was added to the lipid mixture at a concentration of 2 μg/mL in order to fluorescently stain the lipid shell of the PCCAs. The vial was then stoppered and crimped. The vial was purged with 50 mL of a 1:1 mixture of decafluorobutane (DFB) / octafluoropropane (OFP) gases (Fluoromed, Round Rock, TX) via an 18 Gauge needle introduced into the vial septum, along with a vent needle. Mechanical agitation for 45 seconds using a Vialmix™ shaker (Bristol-Myers-Squibb, New York, NY) was sufficient for inducing the formation of stable, microscale bubbles composed of a gaseous perfluorocarbon core encapsulated by a folate-decorated lipid shell.

In order to condense microbubbles into nanodroplets, the headspace of the vial was pressurized according to previously described literature methods [45]. Using a 60 mL syringe and an 18 Gauge needle, 30 mL of room air was compressed into the vial septum while the vial was immersed in an ice-salt bath (−7 °C to −10 °C). A near complete disappearance of large bubbles and a change in the consistency of the PCCA solution indicated successful microbubble condensation. The PCCA solution was kept in the ice-salt bath for 15 minutes to promote nanodroplet formation and stability. PCCA formulations were prepared immediately prior to each individual imaging experiment, such that condensation of microbubbles into nanodroplets preceded incubation with cells by 15 – 20 minutes.

2.3 Confocal Microscopy

Prior to adding PCCAs to the breast cancer cells, 5 μL of Calcein AM dye (Life Technologies, Grand Island, NY) was added to 5 mL media in the tissue culture dish in order to cytoplasmically stain all living cells. Next, 100 μL of PCCA formulation was added to the media in the dish, and cells were incubated at 37 °C for 1 hour. In addition to imaging with FR-targeted PCCAs and untargeted PCCAs, control experiments were performed in which 3 μL DiI (no PCCAs) was added to calcein-stained live cells. Following incubation, media was aspirated and cells were washed with PBS three times to remove any unbound PCCAs from the culture dish. The dish was refilled with 5 mL media for imaging.

One hour prior to imaging, the environmental chamber on the Leica SP5 confocal microscope (Arizona Cancer Center Cancer Imaging Shared Resources) was equilibrated to 37 °C to maintain the live cells for the duration of imaging. An argon 488 nm laser was used to detect calcein ($\lambda_{excitation}$ = 495 nm, $\lambda_{emission}$ = 516 nm), and a HeNe 543 nm laser was

used for DiI ($\lambda_{excitation}$ = 549 nm, $\lambda_{emission}$ = 565 nm). All confocal images were collected using a 63× oil-immersion objective. Z-stacks were obtained as 1-micron sections over a 10 – 12 micron range. Cells were imaged before the application of ultrasound as a baseline. Acoustic activation was achieved using a portable ultrasound unit (ZONARE Medical Systems, Mountain View, CA) with a center US frequency of 9 MHz and a frame rate of 13 Hz. The mechanical index of the acoustic pulse was set to 1.0 or 1.5. The ultrasound transducer was immersed in the culture media and scanned across the dish twice for a total exposure time of 6 seconds. Cells were then imaged immediately after ultrasound exposure.

2.4 Image Analysis and Quantification

Images were analyzed using the LAS AF software that accompanied the Leica SP5 confocal microscope. One culture dish represents one experiment (n = 1), and six experiments (n = 6) were performed for each of the four experimental groups (MDA-MB-231 at MI = 1.0, MDA-MB-231 at MI = 1.5, MCF-7 at MI = 1.0, MCF-7 at MI = 1.5). For each culture dish, images were obtained for 3 – 6 random fields pre-ultrasound and 3 – 6 random fields post-ultrasound. Entire regions of cells were chosen at random regardless of whether microbubbles were present or absent. The entire ensemble of cells was assessed for fluorescently labeled microbubbles, and the average number of microbubbles present per cell was determined both before and after ultrasound activation. Intracellular microbubbles were identified by a circular DiI+ signal (red) that colocalizes with a) a void in the calcein channel and/or b) a bubble in the transmitted light channel. Within the image processing software, all microbubble diameters were manually sized with the software sizing tool. For each dish (pre- and post-US), the proportion of cells with intracellularly activated microbubbles was determined. For all cells with at least 1 intracellular microbubble, the mean number of microbubbles per cell was calculated. Percent internalization and number of intracellular microbubbles per cell values are depicted as mean ± standard error (SE) of the mean. All reported p-values are two-sided.

3. Results

3.1 MDA-MB-231 Imaging

Confocal microscopy imaging of MDA-MB-231 breast cancer cells *in vitro* demonstrated consistent observation of intracellular microbubbles, as evidenced by a red DiI+ signal (Figure 3B) colocalized with a void in the calcein channel (Figure 3A) and/or a bubble in the transmitted light channel (Figure 3C). In total, 1,334 MDA-MB-231 cells were imaged. After the application of ultrasound with MI = 1.0, FR-targeted PCCAs were observed intracellularly in 93.0% ± 2.7% (Mean ± SE) of MDA-MB-231 cells at a rate of 4.38 ± 0.98 (Mean ± SE) microbubbles per cell (Table 1). Parallel MDA-MB-231 imaging experiments were performed at MI = 1.5, with all other conditions held constant. After applying acoustic energy with MI = 1.5, FR-targeted PCCAs were detected intracellularly in 79.5% ± 6.8% (SE) of MDA-MB-231 cells at a rate of 3.63 ± 0.67 (SE) microbubbles per cell (Table 1).

It should be noted that microbubbles were observed intracellularly prior to the application of ultrasound, indicating a thermal component of PCCA activation prior to acoustic droplet vaporization. Before applying ultrasound to MDA-MB-231 cells, FR-targeted microbubbles

were detected intracellularly in 55.2% ± 7.5% (SE) of all cells combined across both acoustic conditions. However, it was clear that after insonation, the proportion of MDA-MB-231 cells with intracellular microbubbles increased significantly ($p < 0.01$) relative to pre-ultrasound data. The ratio of intracellular microbubbles observed post-ultrasound / pre-ultrasound was 1.90 ± 0.32 (SD) using MI = 1.0 and 1.97 ± 0.22 (SD) at MI = 1.5.

In order to confirm that PCCA internalization was occurring via folate receptor-mediated endocytosis, control experiments were conducted using untargeted PCCAs. With all other parameters held constant, PCCAs were formulated without the folate ligand. Confocal imaging of MDA-MB-231 cells using untargeted PCCAs revealed that nonspecific, untargeted uptake of nanodroplets occurs to a minor extent. On average, untargeted PCCAs were observed intracellularly in 4.4% ± 3.0% (SE) of MDA-MB-231 cells after applying ultrasound (Figure 3e). Folate incorporation increased the frequency of intracellular microbubble observation by a factor of roughly 45 compared to untargeted PCCAs. Because folate-decorated PCCAs demonstrated significantly greater uptake than untargeted PCCAs ($p < 0.0001$), this was strong evidence that intracellular PCCA delivery was primarily folate receptor-mediated.

3.2 MCF-7 Imaging

Utilizing the same FR-targeted PCCA formulation, MCF-7 breast cancer cells were imaged to assess intracellular PCCA delivery and activation. In total, 1,525 MCF-7 cells were analyzed. FR-targeted PCCAs were consistently detected intracellularly within MCF-7 cells (Figure 4), albeit significantly less than was observed using MDA-MB-231 cells ($p < 0.001$). After the application of ultrasound with MI = 1.0, FR-targeted PCCAs were observed intracellularly in 42.4% ± 5.0% (SE) of MCF-7 cells at a rate of 1.72 ± 0.07 (SE) microbubbles per cell (Table 1). For the corresponding MCF-7 imaging experiments using MI = 1.5, FR-targeted PCCAs were detected intracellularly in 35.7% ± 6.8% (SE) of cells at a rate of 2.32 ± 0.27 (SE) microbubbles per cell (Table 1).

As was observed during MDA-MB-231 imaging, there were PCCAs vaporized intracellularly within MCF-7 cells before applying ultrasound. Prior to insonation, FR-targeted microbubbles were detected intracellularly in 28.6% ± 3.8% of all MCF-7 cells. Applying acoustic energy with MI = 1.0 increased the frequency of intracellular PCCA observation by a factor of 1.81 ± 0.35 (SD), which indicates that ultrasound at MI = 1.0 significantly amplifies PCCA activation ($p < 0.01$). For the MCF-7 imaging experiments at MI = 1.5, ultrasound application enhanced intracellular PCCA activation by a factor of 1.37 ± 0.35 (SD) ($p = 0.164$).

Control MCF-7 imaging experiments using untargeted PCCAs were performed to quantify nonspecific uptake in comparison to folate receptor-mediated nanoparticle delivery. Without folate incorporation, untargeted PCCAs were observed intracellularly in 8.0% ± 1.0% of MCF-7 cells after insonation (Figure 4e). Decorating the PCCA shell with folate enhanced intracellular delivery significantly ($p < 0.001$). FR-targeted PCCAs were observed intracellularly 8.27 (MI = 1.0) and 5.54 (MI = 1.5) times as frequently as untargeted PCCAs.

3.3 Sizing of Intracellular Microbubbles

Every microbubble detected via microscopy was manually sized with the aforementioned LAS AF software. Across both cell lines, 5,346 microbubbles were identified and sized. Microbubbles observed intracellularly ranged from 500 nm – 6 microns with a skewed right distribution (Figure 5). For MDA-MB-231 imaging experiments, intracellular microbubbles had a mean diameter of 1.09 ± 0.44 (SD) microns with an interquartile range (IQR: defined as the middle 50% of all intracellular microbubble sizes residing between the 25th and 75th percentile) of 0.82 – 1.24 microns (Figure 5). For MCF-7 imaging experiments, the mean size of intracellular microbubbles was 1.29 ± 0.86 (SD) microns with IQR = 0.84 – 1.48 microns (Figure 5).

3.4 Extracellularly Bound Microbubbles

Although the majority of microbubbles were detected intracellularly (93.0% of all MBs observed intracellularly vs. 7.0% extracellularly), there was significant detection of large extracellularly bound microbubbles across both cell lines. Before applying ultrasound, extracellularly bound microbubbles were relatively absent, detected on the surface of less than 1% of all cells. After insonation, microbubbles were observed on the surface of 16.3% of MDA-MB-231 cells and 9.5% of MCF-7 cells. Triplicate PBS washes after the 1-hour incubation period, prior to imaging, ensured that any PCCAs observed extracellularly were bound to surface folate receptors, not simply floating in solution. Extracellular microbubbles ranged from 1 – 100 microns (IQR = 2.2 – 28.3 microns) with a median diameter of 8.7 microns.

4. Discussion

To the best of our knowledge, this is the first demonstration of intracellular delivery and ultrasound-stimulated activation of phase-change contrast agents (PCCAs) targeted to cancer cells. By arming the DPPC / DPPE-PEG lipid shell with folate, we successfully targeted 1:1 DFB/OFP PCCAs to overexpressed folate receptors on the surface of MDA-MB-231 and MCF-7 breast cancer cells. For both cell lines, one hour of incubation proved adequate for PCCA binding and folate receptor-mediated endocytosis.

The unique capabilities of confocal microscopy facilitated reliable intracellular microbubble detection and quantification within live breast cancer cells *in vitro*. The microscope's Z-stack imaging sequence scans the entire three-dimensional volume of each cell, producing fluorescent images that three-dimensionally map DiI+ microbubbles (red) within or outside the calcein+ cytoplasmic regions (green). The intensity and quality of DiI and calcein signals varied between and within samples, but the requirements for positively identifying an intracellular microbubble were held constant: red DiI+ ring (Figure 4B) colocalized with a) void in calcein channel (Figure 4A) and/or b) identifiable bubble in the transmitted light channel (Figure 4C).

For both MDA-MB-231 and MCF-7 cell lines, control experiments incubating with DiI only (no PCCAs) produced no intracellular DiI+ signals (data not included). These results eliminate the possibility that DiI stains intracellular organelles or forms micelles that

internalize. Thus, we verified that any DiI+ rings observed intracellularly are in fact associated with the lipid coat of a PCCA.

Presently, there have been multiple promising Phase II clinical trials using folate receptor-targeted chemotherapeutic agent vintafolide in combination with FR-targeted companion SPECT imaging agent (99m)Tc-etarfolatide for the treatment of ovarian cancer [46, 47]. However, our study may be the first to examine FR-mediated intracellular uptake and activation of a phase-change contrast agent.

Folate receptor-targeted PCCAs were observed intracellularly within both breast cancer cell lines, but cellular uptake was significantly greater for MDA-MB-231 cells ($p < 0.001$). The increased intracellular accumulation of FR-targeted PCCAs in MDA-MB-231 cells (93.0% internalization at MI = 1.0, 79.5% at MI = 1.5) compared to MCF-7 cells (42.4% internalization at MI = 1.0, 35.7% at MI = 1.5) coincides with FR-α expression profiles. MDA-MB-231 cells strongly overexpress FR-α, while FR-α expression is moderate on the surface of MCF-7 cells [34, 35]. Using folate receptor-targeted gold nanoparticles conjugated with doxorubicin, Banu et al. showed that cellular destruction was greater in MDA-MB-231 cells than MCF-7 cells, a reflection of more efficient uptake [39]. Similarly, Meier et al. demonstrated that folate receptor-mediated uptake of iron oxide nanoparticles was significantly greater for MDA-MB-231 cells than MCF-7 cells [34]. It is also possible that other factors, such as the efficiency of endocytosis pathways and passive diffusion mechanisms as well as the expression of other surface receptors, could contribute to the observed difference in PCCA uptake to a minor extent.

Folate receptor-mediated endocytosis was the primary means of PCCA internalization, as indicated by imaging experiments utilizing untargeted PCCAs. Without folate incorporation, roughly 2 – 10% of breast cancer cells showed evidence of intracellular PCCA activation. These results show that nonspecific uptake can occur; however, it occurs infrequently compared to MCF-7 FR-mediated endocytosis ($p < 0.001$) and even less frequently compared to MDA-MB-231 FR-mediated endocytosis ($p < 0.0001$). The increased selectivity of FR-targeted PCCAs toward MDA-MB-231 cells (45-fold greater internalization for FR-targeted vs. untargeted) compared to MCF-7 cells (7-fold greater internalization for FR-targeted vs. untargeted) is notably in agreement with FR-α expression profiles. FR-α overexpression is greater in the MDA-MB-231 cell line than the MCF-7 cell line [34, 35]. Thus, as is consistent with previous literature [34, 39], the uptake-promoting effect of folate decoration is more pronounced when imaging MDA-MB-231 cells.

Other folate receptor-targeted nanoparticles have shown similar evidence of untargeted uptake occurring in addition to FR-mediated delivery. Chen et al. used FR-targeted PLGA nanoparticles to deliver the drug vincristine sulfate intracellularly to MCF-7 cells, and folate incorporation enhanced cytotoxicity by a factor of 1.52 times relative to untargeted nanoparticles carrying the drug [42]. Using MCF-7 cells, Balasundaram et al. showed that folate-armed conjugated polymer nanoparticles produced a photoacoustic signal 5 times that of untargeted nanoparticles [36], which is similar to our MCF-7 data. Utilizing alginate-peptide amphiphile core-shell microparticles to deliver doxorubicin to MDA-MB-231 cells *in vitro*, Boekhoven et al. demonstrated that FR-targeted microparticles produced 60 times

greater cytotoxicity compared to untargeted microparticles [48]. Our MDA-MB-231 imaging showed that folate incorporation increased the frequency of intracellular PCCA detection by roughly 45 times. On the whole, folate receptor targeting appears more favorable for MDA-MB-231 cells than MCF-7 cells, consistent with previous FR-targeted experiments.

The skewed right sizing distribution of intracellular microbubbles (Figure 5) is consistent with previously published sizing data for perfluorocarbon bubbles [19, 24, 26]. The average intracellular microbubble size was 1.09 ± 0.44 (SD) microns for MDA-MB-231 cells and 1.29 ± 0.86 (SD) microns for MCF-7 cells (Figure 5). Using the same 1:1 DFB/OFP perfluorocarbon composition that we employ in the present study, Sheeran et al. described an average microbubble size of 1.02 ± 0.64 (SD) microns with a skewed right distribution due to large outlier bubbles [26]. Thus, the intracellular microbubble size distribution from our *in vitro* study is consistent with the original size distribution profiles from ultrasound-activated PCCAs in solution. The agreement between our weighted distribution of intracellular microbubble sizes (Figure 5) and Sheeran's sizing data [26] indicates that *in vitro* incubation delivers a population of nanodroplets intracellularly capable of yielding microbubbles with sizes similar to microbubbles in solution. It was valuable to ascertain that PCCA condensation, cellular internalization, and vaporization do not substantially alter the distribution of microbubble sizes.

Without directly sizing precursor nanodroplets, the size range of 1:1 DFB/OFP nanodroplets was inferred to lie between 100 – 600 nm, as was previously shown by our group [26]. According to the literature, the maximum nanoparticle size for folate receptor-mediated endocytosis is 400 nm [40, 44]. Assuming approximately 6× volumetric expansion ratio for acoustic droplet vaporization of 1:1 DFB/OFP PCCAs [49, 50], the IQR of intracellularly detected microbubbles (800 nm – 1.5 microns) indicates that the plurality of PCCAs were internalized as nanodroplets ranging from 150 – 250 nm. The smallest intracellular bubbles (500 – 800 nm) likely originated from the vaporization of the smallest nanodroplets (100 – 150 nm). Although the majority of intracellular microbubbles observed were less than 2 microns in diameter, there was occasional detection of larger microbubbles, including some as big as 4 – 6 microns (Figure 5). This population of intracellular microbubbles (2 – 6 microns) may be a product of the largest internalized nanodroplets (250 – 400 nm) and possibly a function of post-vaporization expansion via gas absorption that has been previously described [24].

The appearance of large, extracellularly bound microbubbles after insonation seems to support the concept that there is a maximum nanoparticle size for FR-mediated endocytosis. Of all microbubbles observed, 7.0% were detected extracellularly (median diameter = 8.7 microns). The IQR of extracellular microbubble sizes (2.2 – 28.3 microns) varied significantly ($p < 0.001$) from the IQR of intracellular microbubbles (800 nm – 1.5 microns). Therefore, we hypothesize that extracellular PCCAs are evidence of large outlier nanodroplets (larger than 400 nm) that bind to FR-α yet remain restricted to the extracellular surface. From previously published sizing data for 1:1 DFB/OFP nanodroplets, there is a significant population of droplets larger than 400 nm [26], in other words too large for FR-mediated uptake. Because droplets larger than 400 nm cannot be internalized via FR-mediated endocytosis, these PCCAs are vaporized extracellularly. The polydisperse

distribution of extracellular microbubbles is of marginal consequence for *in vivo* applications because large outlier PCCAs (droplets larger than 600 nm) cannot escape the vasculature. Nevertheless, methods to selectively eliminate large outlier PCCAs should still be considered for future studies. For example, Seo et al. employed microfluidics and a co-solvent approach to control the sizes of perfluorocarbon nanodroplets [51]. Additional methods such as decantation or filtration may be sufficient to eliminate these outliers [28].

Prior to insonation, intracellular microbubbles were detected in approximately 25 – 30 % of MCF-7 cells (Figure 4E) and 50 – 60 % of MDA-MB-231 cells (Figure 3E). The pre-ultrasound detection of intracellularly activated microbubbles can likely be attributed to the vaporization of internalized nanodroplets due to thermal activation. Although 1 hour was provided for PCCA binding and internalization, some literature reports have indicated that folate receptor-mediated nanoparticle uptake can occur in 5 – 10 minutes *in vitro* [52]. Thus, it is possible that a nanodroplet internalized in 10 minutes could lie dormant intracellularly for 1 hour or more before pre-ultrasound imaging. In previously published work from our group, we evaluated the stability of low-boiling perfluorocarbon PCCAs over time. After 1 hour at 37 °C (same temperature used during incubation and imaging for this study), the concentration of 1:1 DFB/OFP nanodroplet samples decreased by 45% due to thermal instability [26]. This seems to support the pre-ultrasound PCCA vaporization observed in our *in vitro* breast cancer imaging study. For future explorations, implementing a less volatile perfluorocarbon mixture that reduces PCCA thermal vaporization may prove valuable. Experiments are in progress using 100% decafluorobutane (DFB, C_4F_{10}) and mixtures of DFB and dodecafluoropentane (DDFP, C_5F_{12}). We do not anticipate PCCA thermal vaporization being overly problematic for *in vivo* applications because thermally activated PCCAs would likely be intravascular, not extravascular, bubbles that will never reach breast cancer tissue due to size constraints.

The mechanical index of ultrasound application was varied in order to determine the vaporization threshold for 1:1 DFB/OFP PCCAs intracellularly. For both breast cancer cell lines, it appears that a mechanical index of 1.0 is sufficient for triggering the vaporization of 1:1 DFB/OFP PCCAs. It must be noted that application of ultrasound was solely for the purposes of activation of internalized PCCAs, while the occurrence of intracellular PCCAs was a function of folate receptor-mediated internalization. Across both cell lines, insonation increased the frequency of intracellular PCCA detection, indicating that ultrasound amplifies the extent of PCCA activation. Ultrasound application significantly increased the occurrence of PCCA vaporization ($p < 0.01$) in three (MDA-MB-231 at MI = 1.0 and 1.5, MCF-7 at MI = 1.0) out of four experimental groups (Table 1). For the MCF-7 group at MI = 1.5, there were more intracellular microbubbles observed after ultrasound activation (Activation Ratio = 1.37 ± 0.35), however the result was insignificant ($p = .164$). Stabilizing the perfluorocarbon mixture and increasing ultrasound exposure time should augment the effect of ultrasonic activation relative to thermal activation. For future studies involving different perfluorocarbon compositions, reassessment of the acoustic activation parameters may prove useful.

With an estimated 40,000 deaths from invasive breast cancer in the United States in 2016 [1], novel methods of early detection and therapy are necessitated. By providing evidence

for the intracellular delivery and activation of folate receptor-targeted PCCAs in breast cancer cells *in vitro*, we hope to expand the scope of exploratory investigation and clinical potential of ultrasound theranostics for breast cancer. For the most part, ultrasound theranostic applications for cancer have remained limited to the vasculature [9, 10, 53, 54], yet the PCCA concept studied herein offers a platform toward extravascular imaging and therapy. Soon, we hope to expand our research to *in vivo* ultrasound imaging of breast cancer tumors in mice.

In addition to intracellular imaging with PCCAs, alternative modes of drug delivery and cellular ablation are possible by manipulating the acoustic parameters to induce microbubble cavitation. Using dodecafluoropentane (DDFP) emulsion-loaded liposomes targeted to MCF-7 cells, Ninomiya et al. provided evidence for ultrasound-mediated cell rupture, resulting in 43% cell viability after insonation [55]. Conjugation of a nuclear localization sequence [56] to the PCCA shell can promote migration of intracellular nanoparticles to the nucleus, thereby maximizing ultrasound-mediated therapeutic effects. Although PCCA research remains in its early stages, we are hopeful that the data presented in this study facilitates a new outlook on ultrasound molecular imaging and therapy.

Acknowledgments

This work was supported by National Institutes of Health grant no. R21CA185684 (to T.O.M.). The authors' also acknowledge the use of the confocal microscope operated by the Tissue Acquisition and Cellular/Molecular Analysis Shared Resource (TACMASR) facility supported by the University of Arizona Cancer Center Support Grant, NIH CA023074.

Common Abbreviations

PCCA	phase-change contrast agent
US	ultrasound
MB	microbubble
PFC	perfluorocarbon
BP	boiling point
DFB	decafluorobutane
OFP	octafluoropropane
DDFP	dodecafluoropentane
MI	mechanical index
FR	folate receptor
IQR	interquartile range
SD	standard deviation
SE	standard error

References

1. Breast Cancer Facts and Figures 2015 – 2016. American Cancer Society. <www.cancer.org>.
2. Eccles SA, Aboagye EO, Anderson AS, Gee JM, Young LS, Thompson AM. Critical research gaps and translational priorities for the successful prevention and treatment of breast cancer. Breast Cancer Research. 2013; 15(5):R92. [PubMed: 24286369]
3. Deshpande N, Needles A, Willmann JK. Molecular ultrasound imaging: current status and future directions. Clinical Radiology. 2010; 65(7):567–581. [PubMed: 20541656]
4. Rix A, Palmowski M, Kiessling F. Molecular ultrasound imaging: clinical applications. Radiologe. 2015; 55(11):956–963. [PubMed: 26438094]
5. Hoyt K, Umphrey H, Lockhart M, Robbin M, Forero-Torres A. Ultrasound imaging of breast tumor perfusion and neovascular morphology. Ultrasound in Medicine and Biology. 2015; 41(9):2292–2302. [PubMed: 26116159]
6. Koonce NA, Levy J, Hardee ME, Jamshidi-Parsian A, Vang KB, Sharma S, Raleigh JA, Dings R, Griffin RJ. Targeting artificial tumor stromal targets for molecular imaging of tumor vascular hypoxia. PLoS One. 2015; 10(8):e0135607. [PubMed: 26308944]
7. Bachawal SV, Jensen KC, Wilson KE, Tian L, Lutz AM, Willmann JK. Breast cancer detection by B7-H3-targeted ultrasound molecular imaging. Cancer Research. 2015; 75(12):2501–2509. [PubMed: 25899053]
8. Hernot S, Klibanov AL. Microbubbles in ultrasound-triggered drug and gene delivery. Advanced Drug Delivery Reviews. 2008; 60(10):1153–1166. [PubMed: 18486268]
9. Geis NA, Katus HA, Bekeredjian R. Microbubbles as a vehicle for gene and drug delivery: current clinical implications and future perspectives. Current Pharmaceutical Design. 2012; 18(15):2166–2183. [PubMed: 22352771]
10. Khokhlova TD, Haider Y, Hwang JH. Therapeutic potential of ultrasound microbubbles in gastrointestinal oncology: recent advances and future prospects. Therapeutic Advances in Gastroenterology. 2015; 8(6):384–394. [PubMed: 26557894]
11. Shim CY, Liu YN, Atkinson T, Xie A, Foster T, Davidson BP, Treible M, Qi Y, Lopez JA, Munday A, Ruggeri Z, Lindner JR. Molecular imaging of platelet-endothelial interactions and endothelial von Willebrand factor in early and mid-stage atherosclerosis. Circulation: Cardiovascular Imaging. 2015; 8(7):e002765. [PubMed: 26156014]
12. Streeter JE, Gessner RC, Tsurutu J, Feingold S, Dayton PA. Assessment of molecular imaging of angiogenesis with three-dimensional ultrasonography. Molecular Imaging. 2011; 10(6):460–468. [PubMed: 22201537]
13. Knowles JA, Heath CH, Saini R, Umphrey H, Warram J, Hoyt K, Rosenthal EL. Molecular targeting of ultrasonographic contrast agent for detection of head and neck squamous cell carcinoma. Archives of Otolaryngology- Head and Neck Surgery. 2012; 138(7):662–668. [PubMed: 22801891]
14. Kripfgans OD, Fowlkes JB, Miller DL, Eldevik OP, Carson PL. Acoustic droplet vaporization for therapeutic and diagnostic applications. Ultrasound in Medicine and Biology. 2000; 26(7):1177–1189. [PubMed: 11053753]
15. Ernsting MJ, Murakami M, Roy A, Li SD. Factors controlling the pharmacokinetics, biodistribution and intratumoral penetration of nanoparticles. Journal of Controlled Release. 2013; 172(3):782–794. [PubMed: 24075927]
16. Chen F, Cai W. Tumor vasculature targeting: a generally applicable approach for functionalized nanomaterials. Small. 2014; 10(10):1887–1893. [PubMed: 24591109]
17. Ji T, Zhao Y, Ding Y, Nie G. Using functional nanomaterials to target and regulate the tumor microenvironment: diagnostic and therapeutic applications. Advanced Materials. 2013; 25(26): 3509–3525.
18. Sheeran PS, Rojas JD, Puett C, Hjelmquist J, Arena CB, Dayton PA. Contrast-enhanced ultrasound imaging and in vivo circulatory kinetics with low-boiling-point nanoscale phase-change perfluorocarbon agents. Ultrasound in Medicine and Biology. 2015; 41(3):814–831. [PubMed: 25619781]

19. Matsunaga TO, Sheeran PS, Louis S, Streeter JE, Mullin LB, Banerjee B, Dayton PA. Phase-change nanoparticles using highly volatile perfluorocarbons: toward a platform for extravascular ultrasound imaging. Theranostics. 2012; 2(12):1185–1198. [PubMed: 23382775]
20. Mountford PA, Thomas AN, Borden MA. Thermal activation of superheated lipid-coated perfluorocarbon drops. Langmuir. 2015; 31(16):4627–4634. [PubMed: 25853278]
21. Definity Prescriber Information for Intravenous Use. Lantheus Medical Imaging. www.definityimaging.com/pdf/DEFINITY_US_PI_MKTG_515987-0813.pdf.
22. Sheeran PS, Dayton PA. Phase-change contrast agents for imaging and therapy. Current Pharmaceutical Design. 2012; 18(15):2152–2165. [PubMed: 22352770]
23. Porter TR, Arena C, Sayyed S, Lof J, High RR, Xie F, Dayton PA. Targeted transthoracic acoustic activation of systematically administered nanodroplets to detect myocardial perfusion abnormalities. Circulation Cardiovascular Imaging. 2016; 9(1):e003770. pii. [PubMed: 26712160]
24. Sheeran PS, Streeter JE, Mullin L, Matsunaga TO, Dayton PA. Toward ultrasound molecular imaging with phase-change contrast agents: an in vitro proof of principle. Ultrasound in Medicine and Biology. 2013; 39(5):893–902. [PubMed: 23453380]
25. Sheeran PS, Wong VP, Louis S, McFarland RJ, Ross WD, Feingold S, Matsunaga TO, Dayton PA. Decafluorobutane as a phase-change contrast agent for low-energy extravascular ultrasonic imaging. Ultrasound in Medicine and Biology. 2011; 37(9):1518–1530. [PubMed: 21775049]
26. Sheeran PS, Louis S, Mullin L, Matsunaga TO, Dayton PA. Design of ultrasonically-activatable nanoparticles using low boiling point perfluorocarbons. Biomaterials. 2012; 33(11):3262–3269. [PubMed: 22289265]
27. Sheeran PS, Matsunaga TO, Dayton PA. Phase-transition thresholds and vaporization phenomena for ultrasound phase-change nanoemulsions assessed via high-speed optical microscopy. Physics in Medicine and Biology. 2013; 58(13):4513–4523. [PubMed: 23760161]
28. Sheeran PS, Daghighi Y, Yoo K, Williams R, Cherin E, Foster FS, Burns PN. Image-guided ultrasound characterization of volatile sub-micron phase-shift droplets in the 20–40 MHz frequency range. Ultrasound in Medicine and Biology. 2016; 42(3):795–807. [PubMed: 26725168]
29. Parker N, Turk MJ, Westrick E, Lewis JD, Low PS, Leamon CP. Folate receptor expression in carcinomas and normal tissues determined by a quantitative radioligand binding assay. Analytical Biochemistry. 2005; 338(2):284–293. [PubMed: 15745749]
30. Zhang Z, Wang J, Tacha DE, Li P, Bremer RE, Chen H, Wei B, Xiao X, Da J, Skinner K, Hicks DG, Bu H, Tang P. Folate receptor alpha associated with triple-negative breast cancer and poor prognosis. Archives of Pathology and Laboratory Medicine. 2014; 138(7):890–895. [PubMed: 24028341]
31. Hartmann LC, Keeney GL, Lingle WL, Christianson TJ, Varghese B, Hillman D, Oberg AL, Low PS. Folate receptor overexpression is associated with poor outcome in breast cancer. International Journal of Cancer. 2007; 121(5):938–942. [PubMed: 17487842]
32. Necela BM, Crozier JA, Andorfer CA, Lewis-Tuffin L, Kachergus JM, Geiger XJ, Kalari KR, Serie DJ, Sun Z, Aspita AM, O'Shannessy DJ, Maltzman JD, McCullough AE, Pockaj BA, Cunliffe HE, Ballman KV, Thompson EA, Perez EA. Folate receptor-α (FOLR1) expression and function in triple negative tumors. PLoS One. 2015; 10(3):e0122209. [PubMed: 25816016]
33. Xu S, Olenyuk BZ, Okamoto CT, Hamm-Alvarez SF. Targeting receptor-mediated endocytotic pathways with nanoparticles: rationale and advances. Advanced Drug Delivery Reviews. 2013; 65(1):121–138. [PubMed: 23026636]
34. Meier R, Henning TD, Boddington S, Tavri S, Arora S, Piontek G, Rudelius M, Corot C, Daldrup-Link HE. Breast cancers: MR imaging of folate-receptor expression with the folate-specific nanoparticle P1133. Radiology. 2010; 255(2):527–535. [PubMed: 20413763]
35. Yang T, Xu F, Fang D, Chen Y. Targeted proteomics enables simultaneous quantification of folate receptor isoforms and potential isoform-based diagnostics in breast cancer. Scientific Reports. 2015; 5:16733. [PubMed: 26573433]
36. Balasundaram G, Ho CJ, Li K, Driessen W, Dinish US, Wong CL, Ntziachristos V, Liu B, Olivo M. Molecular photoacoustic imaging of breast cancer using an actively targeted conjugated polymer. International Journal of Nanomedicine. 2015; 10:387–397. [PubMed: 25609951]

37. Li H, Miteva M, Kirkbride KC, Cheng MJ, Nelson CE, Simpson EM, Gupta MK, Duvall CL, Giorgio TD. Dual MMP7-proximity-activated and folate receptor-targeted nanoparticles for siRNA delivery. Biomacromolecules. 2015; 16(1):192–201. [PubMed: 25414930]

38. Lu PL, Chen YC, Ou TW, Chen HH, Tsai HC, Wen CJ, Lo CL, Wey SP, Lin KJ, Yen TC, Hsiue GH. Multifunctional hollow nanoparticles based on graft-diblock copolymers for doxorubicin delivery. Biomaterials. 2011; 32(8):2213–2221. [PubMed: 21176954]

39. Banu H, Sethi DK, Edgar A, Sheriff A, Rayees N, Renuka N, Faheem SM, Premkumar K, Vasanthakumar G. Doxorubicin loaded polymeric gold nanoparticles targeted to human folate receptor upon laser photothermal therapy potentiates chemotherapy in breast cancer cell lines. Journal of Photochemistry and Photobiology. 2015; 149:116–128.

40. Wang F, Chen Y, Zhang D, Zhang Q, Zheng D, Hao L, Liu Y, Duan C, Jia L, Liu G. Folate-mediated targeted and intracellular delivery of paclitaxel using a novel deoxycholic acid-O-carboxymethylated chitosan-folic acid micelles. International Journal of Nanomedicine. 2012; 7:325–337. [PubMed: 22287842]

41. Satsangi A, Roy SS, Satsangi RK, Tolcher AW, Vadlamudi RK, Goins B, Ong JL. Synthesis of a novel, sequentially active-targeted drug delivery nanoplatform for breast cancer therapy. Biomaterials. 2015; 59:88–101. [PubMed: 25956854]

42. Chen J, Li S, Shen Q, He H, Zhang Y. Enhanced cellular uptake of folic acid-conjugated PLGA-PEG nanoparticles loaded with vincristine sulfate in human breast cancer. Drug Development and Industrial Pharmacy. 2011; 37(11):1339–1346. [PubMed: 21524153]

43. Javadi M, Pitt WG, Tracy CM, Barrow JR, Willardson BM, Hartley JM, Tsosie NH. Ultrasonic gene and drug delivery using eLiposomes. Journal of Controlled Release. 2013; 167(1):92–100. [PubMed: 23352908]

44. Nahire R, Haldar MK, Paul S, Ambre AH, Meghani V, Layek B, Katti KS, Gange KN, Singh J, Sarkar K, Mallik S. Multifunctional polymersomes for cytosolic delivery of gemcitabine and doxorubicin to cancer cells. Biomaterials. 2015; 35(24):6482–6497.

45. Sheeran PS, Louis S, Dayton PA, Matsunaga TO. Formulation and acoustic studies of a new phase-shift agent for diagnostic and therapeutic ultrasound. Langmuir. 2011; 27(17):10412–10420. [PubMed: 21744860]

46. Naumann RW, Coleman RL, Burger RA, Sausville EA, Kutarska E, Ghamanda SA, Gabrail NY, Depasquale SE, Nowara E, Gilbert L, Gersh RH, Teneriello MG, Harb WA, Konstantinopoulos PA, Penson RT, Symanowski JT, Lovejoy CD, Leamon CP, Morgenstern DE, Messmann RA. Precendent: a randomized phase II trial comparing vintafolide (EC145) and pegylated liposomal doxorubicin (PLD) in combination versus PLD alone in patients with platinum-resistant ovarian cancer. Journal of Clinical Oncology. 2013; 31(35):4400–4406. [PubMed: 24127448]

47. Morris RT, Joyrich RN, Naumann RW, Shah NP, Maurer AH, Strauss HW, Uszier JM, Symanowski JT, Ellis PR, Harb WA. Phase II study of treatment of advanced ovarian cancer with folate-receptor-targeted therapeutic (vintafolide) and companion SPECT-based imaging agent (99mTc-etarfolatide). Annals of Oncology. 2014; 25(4):852–858. [PubMed: 24667717]

48. Boekhoven J, Zha RH, Tantakitti F, Zhuang E, Zandi R, Newcomb CJ, Stupp SI. Alignate-peptide amphiphile core-shell microparticles as a targeted drug delivery system. RSC Advances. 2015; 5(12):8752–8756.

49. Lin CY, Pitt WG. Acoustic droplet vaporization in biology and medicine. Biomedical Research International. 2013:e404361.

50. Doinikov AA, Sheeran PS, Bouakaz A, Dayton PA. Vaporization dynamics of volatile perfluorocarbon droplets: a theoretical model and in vitro validation. Medical Physics. 2014; 41(10):102901. [PubMed: 25281982]

51. Seo M, Williams R, Matsuura N. Size reduction of cosolvent-infused microbubbles to form acoustically responsive monodisperse perfluorocarbon nanodroplets. Lab on a Chip. 2015; 15(17): 3581–3590. [PubMed: 26220563]

52. Prokop A, Davidson JM. Nanovehicular intracellular delivery systems. Journal of Pharmaceutical Sciences. 2008; 97(9):3518–3590. [PubMed: 18200527]

53. Rapoport N, Nam KH, Gupta R, Gao Z, Mohan P, Payne A, Todd N, Liu X, Kim T, Shea J, Scaife C, Parker DL, Jeong EK, Kennedy AM. Ultrasound-mediated tumor imaging and nanotherapy

using drug loaded, block copolymer stabilized perfluorocarbon nanoemulsions. Journal of Controlled Release. 2011; 153(1):4–15. [PubMed: 21277919]

54. Czarnota GJ. Ultrasound-stimulated microbubble enhancement of radiation response. Biological Chemistry. 2015; 396(6):645–657. [PubMed: 25741736]
55. Ninomiya K, Yamashita T, Tanabe Y, Imai M, Takahashi K, Shimizu N. Targeted and ultrasound-triggered cancer cell injury using perfluorocarbon emulsion-loaded liposomes endowed with cancer cell-targeteing and fusogenic capabilities. Ultrasonics Sonochemistry. 2016; 28:54–61. [PubMed: 26384883]
56. Wang HY, Li C, Yi WJ, Sun YX, Cheng SX, Zhuo RX, Zhang XZ. Targeted delivery in breast cancer cells via iodine: nuclear localization sequence conjugate. Bioconjugate Chemistry. 2011; 22(8):1567–1575. [PubMed: 21688833]

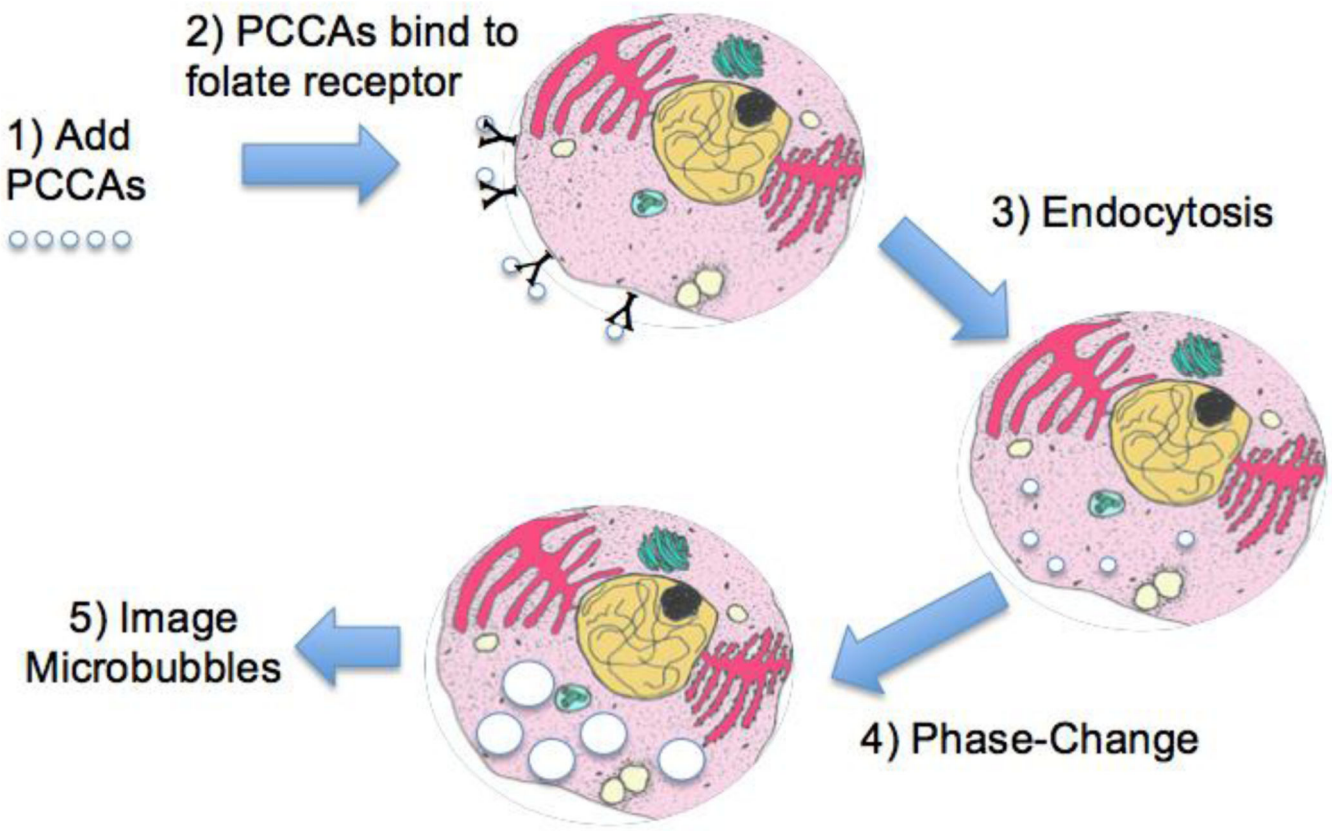

Figure 1.

Schematic illustration of *in vitro* breast cancer imaging: (1) Liquid perfluorocarbon phase-change contrast agents (PCCAs) added directly to culture medium for 1-hour incubation. (2) Folate-decorated PCCAs bind to folate receptors overexpressed on the surface of breast cancer cells. (3) PCCA nanodroplets internalize via folate receptor-mediated endocytosis. (4) Ultrasound pulse triggers phase-shift from liquid nanodroplets to gaseous microbubbles. (5) Intracellularly activated microbubbles imaged via confocal microscopy.

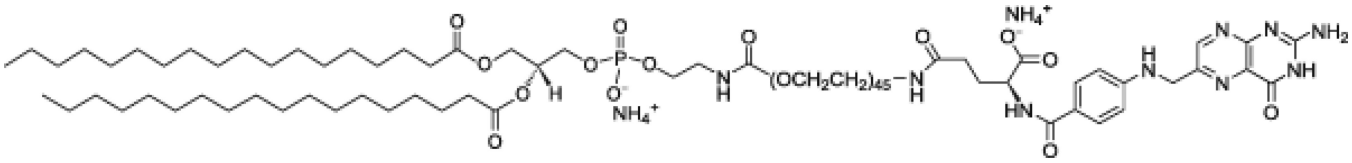

Figure 2.

Chemical structure of the folate targeting construct: 1,2-distearoyl-*sn*-glycero-3-phosphoethanolamine-N-[folate(polyethylene glycol)-2000] (ammonium salt) (DSPE-PEG(2000) Folate)

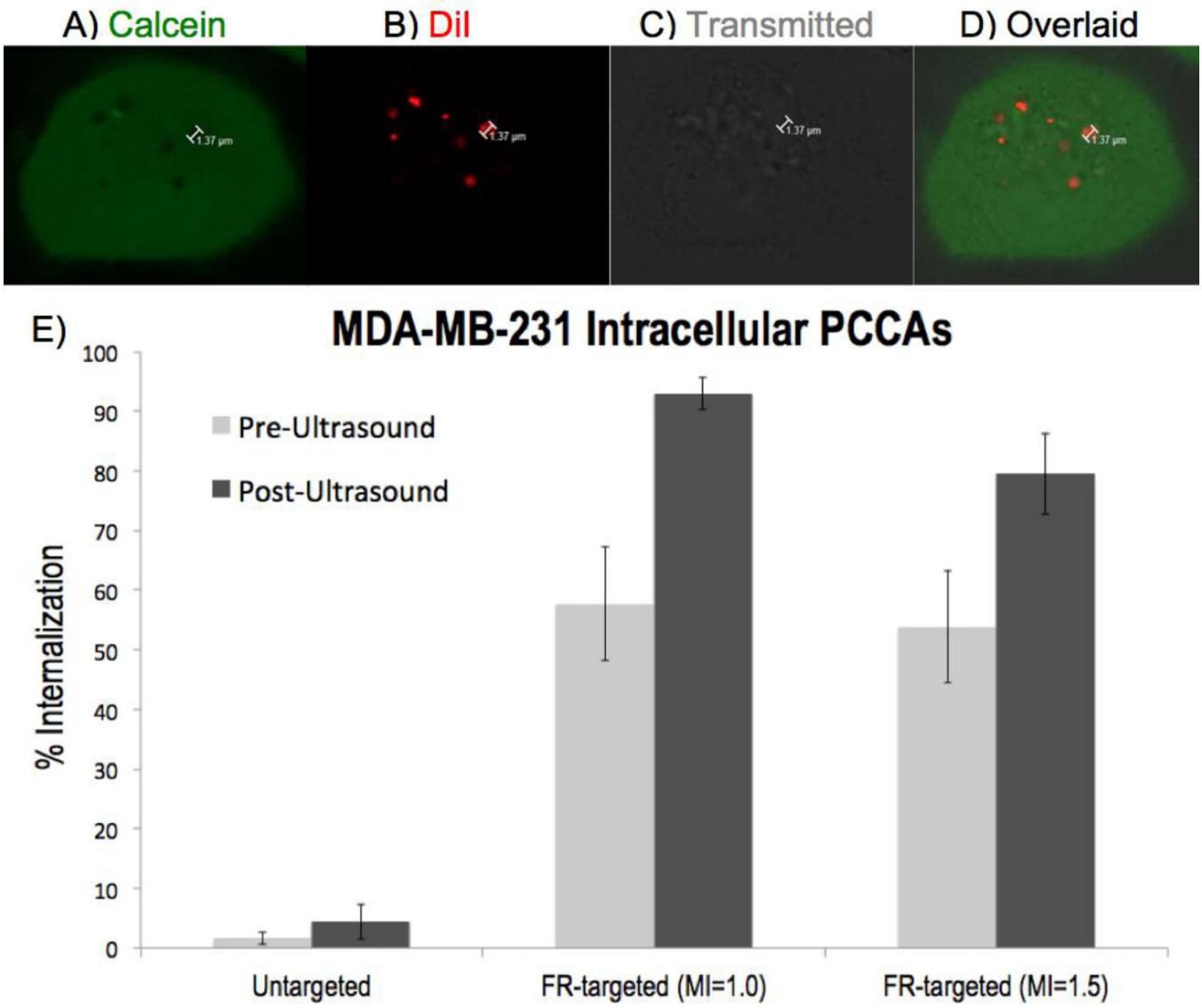

Figure 3.

MDA-MB-231 intracellular imaging, with top row (A–D) depicting 7 FR-targeted PCCAs activated intracellularly after insonation at MI = 1.0 (A) Calcein stains the cytoplasm of living cells. (B) DiI stains the lipid shell of PCCAs. (C) Transmitted light channel shows bubble-like structures intracellularly. (D) All three channels overlaid shows the colocalization of DiI+ / calcein- regions. (E) Graph depicts the proportion of MDA-MB-231 cells (mean +/− SE) with at least 1 intracellularly activated microbubble before (left, light gray) and after (right, dark gray) ultrasound application.

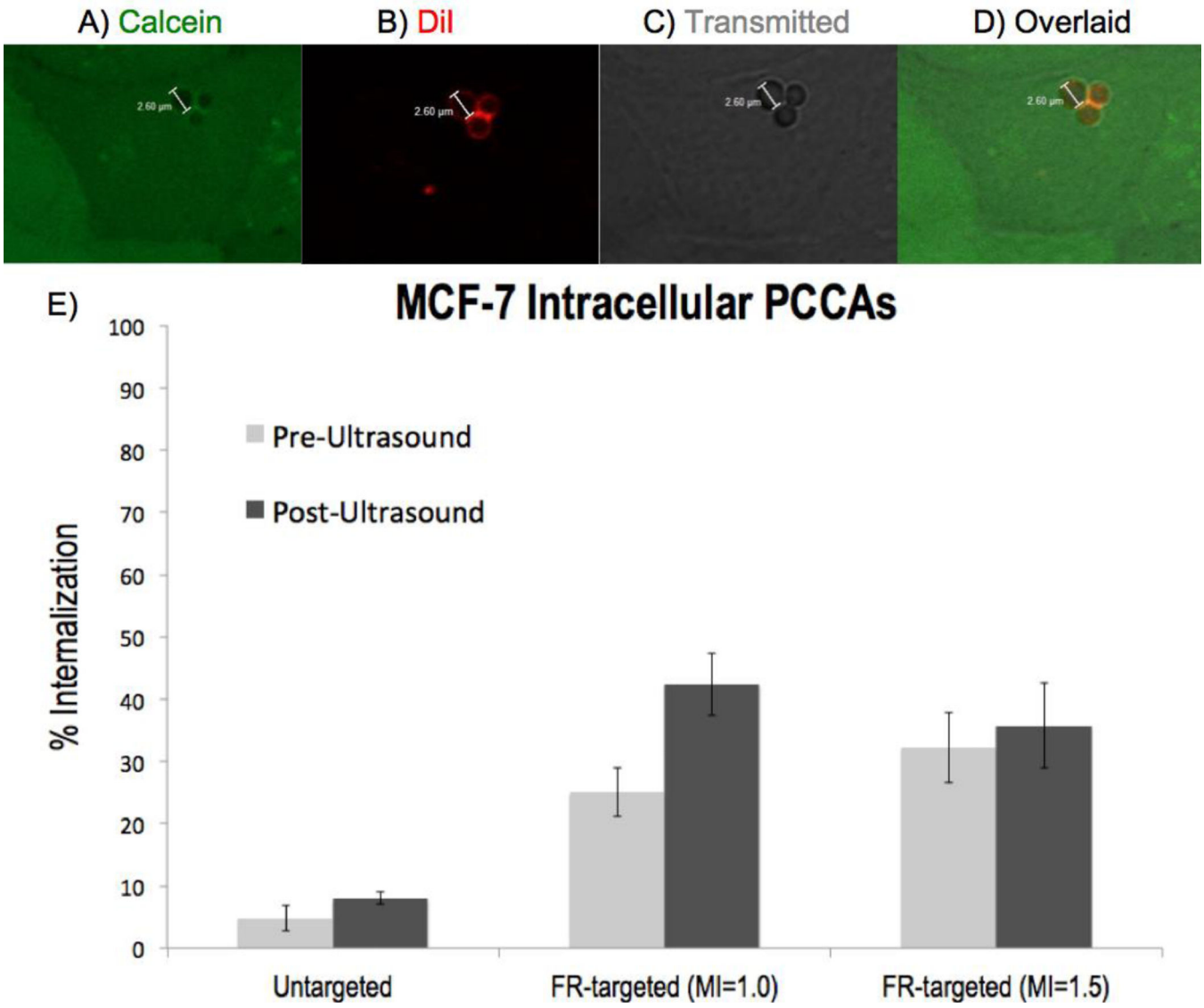

Figure 4.

MCF-7 intracellular imaging, with top row (A–D) depicting 3 intracellular FR-targeted PCCAs after insonation at MI = 1.5 (A) Cytoplasmic stain calcein shows 3 circular voids. (B) DiI stains the lipid shell of PCCAs. (C) Transmitted light channel shows 3 bubbles intracellularly. (D) All three channels overlaid shows the colocalization of DiI+ / calcein- bubble regions. (E) Graph depicts the proportion of MCF-7 cells (mean +/− SE) with at least 1 intracellularly activated microbubble before (left, light gray) and after (right, dark gray) ultrasound application.

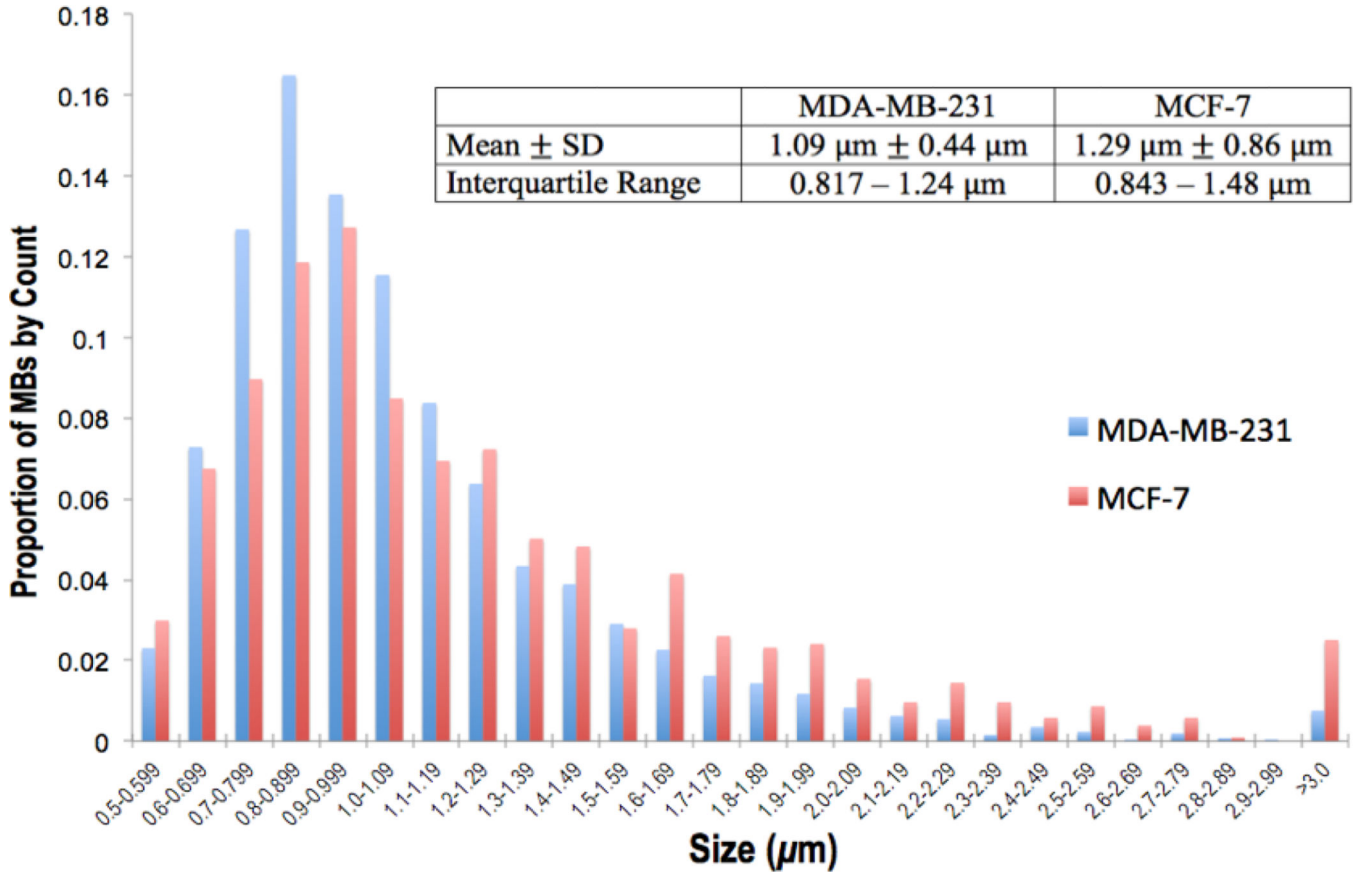

Figure 5.

Sizing of intracellular microbubbles (MBs) detected within MDA-MB-231 cells (left, blue) and MCF-7 cells (right, red)

Table 1

Summary statistics for MDA-MB-231 (n = 6 at MI = 1.0, n = 6 at MI = 1.5) and MCF-7 (n = 6 at MI = 1.0, n = 6 at MI = 1.5) imaging experiments. (i) % Internalization = percentage of cells with at least 1 intracellular microbubble. (ii) # MB per cell = mean number of microbubbles per cell, for all cells with at least 1 intracellular microbubble. (iii) Ultrasound Activation Ratio = number of intracellular microbubbles per cell post-ultrasound / number of intracellular microbubbles per cell pre-ultrasound, including those cells with 0 intracellular PCCAs. (iv) FR-α Targeting Ratio = number of FR-targeted intracellular microbubbles per cell / number of untargeted intracellular microbubbles per cell, including those cells with 0 intracellular PCCAs.

Cell Line	**MDA-MB-231**		**MCF-7**	
Mechanical Index	MI = 1.0	MI = 1.5	MI = 1.0	MI = 1.5
i) % Internalization (± SE)	93.0% ± 2.7%	79.5% ± 6.8%	42.4% ± 5.0%	35.7% ± 6.8%
ii) # MB per cell (± SE)	4.38 ± 0.98	3.63 ± 0.67	1.72 ± 0.07	2.32 ± 0.27
iii) Ultrasound Activation Ratio (± SD)	1.90 ± 0.32 ($p < 0.01$)	1.97 ± 0.22 ($p < 0.01$)	1.81 ± 0.35 ($p < 0.01$)	1.37 ± 0.33 ($p = 0.164$)
iv) FR-α Targeting Ratio	44.8 ($p < 0.0001$)	48.5 ($p < 0.0001$)	8.27 ($p < 0.001$)	5.54 ($p < 0.001$)